Planetary and Space Science 85 (2013) 78–88

Contents lists available at ScienceDirect

Planetary and Space Science

journal homepage: www.elsevier.com/locate/pss

Nighttime photochemical model and night airglow on Venus

Vladimir A. Krasnopolsky *

[a] Department of Physics, Catholic University of America, Washington, DC 20064, USA
[b] Moscow Institute of Physics and Technology, Dolgoprudnyy 141700 Russia

ARTICLE INFO

Article history:
Received 23 December 2012
Received in revised form
28 April 2013
Accepted 31 May 2013
Available online 18 June 2013

Keywords:
Venus
Photochemistry
Night airglow
Atmospheres
Composition
Atmospheres
Chemistry

ABSTRACT

The photochemical model for the Venus nighttime atmosphere and night airglow (Krasnopolsky, 2010, Icarus 207, 17–27) has been revised to account for the SPICAV detection of the nighttime ozone layer and more detailed spectroscopy and morphology of the OH nightglow. Nighttime chemistry on Venus is induced by fluxes of O, N, H, and Cl with mean hemispheric values of 3×10^{12}, 1.2×10^{9}, 10^{10}, and 10^{10} cm^{-2} s^{-1}, respectively. These fluxes are proportional to column abundances of these species in the daytime atmosphere above 90 km, and this favors their validity. The model includes 86 reactions of 29 species. The calculated abundances of Cl_2, ClO, and $ClNO_3$ exceed a ppb level at 80–90 km, and perspectives of their detection are briefly discussed. Properties of the ozone layer in the model agree with those observed by SPICAV. An alternative model without the flux of Cl agrees with the observed O_3 peak altitude and density but predicts an increase of ozone to 4×10^{8} cm^{-3} at 80 km. Reactions H+O_3 and O+HO_2 that may excite the OH nightglow have equal column rates. However, the latter is shifted to 92–94 km, and the models agree better with the nightglow observations if O+HO_2 does not contribute to the OH excitation. Schemes for quenching of the OH vibrational quanta by CO_2 are chosen to fit the observed band distribution in the $\Delta v=1$ sequence at 2.9 μm. The models agree with all observational constraints for the mean nighttime atmosphere. Analytic relationships between the nightglow intensities, the ozone layer, and the input fluxes of atomic species are given. The model results are compared with those of three-dimensional models for the Venus thermosphere.

1. Introduction

Night airglow is an interesting phenomenon and a convenient tracer of chemical and dynamical processes in the lower thermosphere of Venus. Since its discovery in the visible range by the Venera 9 and 10 orbiters (Krasnopolsky et al., 1976; Krasnopolsky, 1983a), the UV nightglow of the NO γ and δ bands was detected using the International Ultraviolet Explorer (Feldman et al., 1979) and then studied from the Pioneer Venus orbiter (Stewart et al., 1980). Ground-based observations resulted in detection of the nightglow of the O_2 band at 1.27 μm (Connes et al., 1979) and the O green line at 558 nm (Slanger et al., 2001).

The most detailed observations of the Venus nightglow were made using the Venus Express orbiter. Morphology of the O_2 nightglow at 1.27 μm (Piccioni et al., 2009) and in the visible range (Garcia Munoz et al., 2009a; Migliorini et al., 2013) as well as that of the NO UV nightglow (Gerard et al., 2008) have been studied. New emissions discovered at the Venus night side are the NO ($C^2\Pi\rightarrow A^2\Sigma^+$) band at 1.224 μm (Garcia Munoz et al., 2009b) and the OH rovibrational bands (Piccioni et al.,2008). The OH emissions in two bands were also observed from the ground (Krasnopolsky, 2010). The O_2 and NO nightglow emissions and their mean nightside intensities are listed in Table 1; those of OH will be discussed later. A problem of excitation, energy transfer, and quenching of the oxygen emissions in the nightglows of the Earth, Venus, and Mars was considered by Krasnopolsky (2011). That paper combined the observational data on the vertical profiles of all O_2 band systems in the nightglow on the Earth and Venus with laboratory and theoretical data on the O_2 excitation, quenching, and energy transfer and suggested a scheme for these processes that compromises and fits to all existing data (Table 2).

To respond to the observed basic O_2, NO, and OH nightglows, their mean intensities and vertical profiles, a photochemical model for the nighttime atmosphere of Venus at 80–130 km has been developed (Krasnopolsky, 2010; hereafter Kr10). The model involves oxygen, hydrogen, chlorine, and nitrogen chemistries with fluxes of O, N, and H at the upper boundary as input parameters. The model results were in excellent agreement with the observational data available at that time.

However, stellar occultations using SPICAV at Venus Express revealed a high-altitude ozone layer in the nighttime atmosphere of Venus (Montmessin et al., 2011). Properties of the ozone layer are variable with the following mean values: peak altitude is

* Tel.: +1 240 473 6831.
E-mail address: vlad.krasn@verizon.net

0032-0633/$ - see front matter © 2013 Elsevier Ltd. All rights reserved.
http://dx.doi.org/10.1016/j.pss.2013.05.022

Table 1
O, O_2, and NO night airglow on Venus.

Emission	Name	λ	Intensity (R)
$O(^1S \rightarrow {}^1D)$	Green line	558 nm	≤15[a]
$O_2(A^3\Sigma_u^+ \rightarrow X^3\Sigma_g^-)$	Herzberg I system	380–530 nm	140[b]
$O_2(A'^3\Delta_u \rightarrow a^1\Delta_g)$	Chamberlain system	520–720 nm	200[b]
$O_2(c^1\Sigma_u^- \rightarrow X^3\Sigma_g^-)$	Herzberg II system	400–650 nm	2700[b,c]
$O_2(a^1\Delta_g \rightarrow X^3\Sigma_g^-)$	IR Atmospheric system	1.27, 1.58 μm	0.5 MR[d]
$NO(C^2\Pi(v=0) \rightarrow X^2\Pi)$	δ-System	190–230 nm	270[e]
$NO(C^2\Pi(v=0) \rightarrow A^2\Sigma^+(v=0))$	Heath band	1.224 μm	130[e,f]
$NO(A^2\Sigma^+(v=0) \rightarrow X^2\Pi)$	γ-System	230–260 nm	130[e]

[a] Observed only during some ionospheric events (Slanger et al., 2006; Fox, 2012).
[b] Krasnopolsky (1983a).
[c] Garcia Munoz et al. (2009a).
[d] Piccioni et al. (2009).
[e] Based on Gerard et al. (2008) and discussion in Krasnopolsky (2010).
[f] Garcia Munoz et al. (2009b).

Table 2
Excitation, excitation transfer, and quenching processes in the O_2 nightglow.

State	Bands	τ (s)	α	α_{TE}	α_{TV}	k_O	k_{O_2}	k_{N_2}	k_{CO_2}
$A^3\Sigma_u^+$	HzI	0.14	0.04	0	0	1.3×10^{-11}	4.5×10^{-12}	3×10^{-12}	8×10^{-12}
$A'^3\Delta_u$	Chm	2–4	0.12	0	0	1.3×10^{-11}	3.5×10^{-12}	2.3×10^{-12}	4.5×10^{-13}
$c^1\Sigma_u^-$	HzII	5–7	0.03	0	0	8×10^{-12}	$3\times10^{-14}/1.8\times10^{-11}$	–	1.2×10^{-16}
$b^1\Sigma_g^+$	762 nm	13	0.02	0.09	0.125	8×10^{-14}	4×10^{-17}	2.5×10^{-15}	3.4×10^{-13}
$a^1\Delta_g$	1.27 μm	4460	0.05	0.35	0.65	–	10^{-18}	$<10^{-20}$	10^{-20}

HzI, HzII, and Chm are the Herzberg I, II, and Chamberlain bands; τ is the radiative lifetime; if two values are given, then they refer to high and low vibrational excitation on the Earth and Venus, respectively; α is the direct excitation yield; αTE and αTV are excitation transfer yields for Earth and Venus from the upper states including 5Πg (see details in Krasnopolsky (2011)); and k_X are quenching rate coefficients in $cm^3\ s^{-1}$. Two values of k_{O_2} are for $c^1\Sigma_g^+$ ($v=0$ and 7–11). From Krasnopolsky (2011).

≈95 km, peak density is $\approx 7\times10^7\ cm^{-3}$, and full width at half maximum (FWHM) is ≈7 km. The model by Kr10 predicted an ozone layer at 94 km with a similar width but with a peak density of $4\times10^9\ cm^{-3}$, exceeding that observed by a factor of 60. The observed O_3 density is close to that in a global-mean photochemical model for Venus (Krasnopolsky, 2012) that gives $[O_3]=7\times10^7\ cm^{-3}$ at 92 km. However, the O_3 photolysis rate is half a daytime value in the global-mean model and significantly depletes ozone; therefore ozone in the daytime and global-mean models is inapplicable to the nighttime conditions. The results of Montmessin et al. (2011) look convincing and indicate that the model in Kr10 needs a revision. This is a basic goal of this paper. Furthermore, the much smaller ozone abundances and new data on the OH band distribution (Soret et al., 2012) require significant adjustments in the model of excitation and quenching of OH on Venus. This is another goal of this work.

2. Observations of the OH nightglow on Venus

The OH nightglow on Venus was discovered using the VIRTIS-M-IR spectrograph at the Venus Express orbiter (Piccioni et al., 2008). The nightglow is maximum near the antisolar point (midnight at low latitudes), and spectral sequences $\Delta v=v'-v''=1$ and 2 at 2.9 and 1.4 μm were detected with peak limb intensities of 880 ± 90 kR and 100 ± 40 kR, respectively, at 96 ± 2 km near the antisolar point. (One Rayleigh is 10^6 photons per cm^2, s, and 4π sr.) We convert limb intensities into vertical intensities using air mass $\beta=(8(R+h)/d)^{1/2}$. Here $R=6052$ km is the planet radius, h is the airglow altitude, and d is the airglow layer thickness. The Venus Express observations and Kr10 give $d\approx15$ km as full widths at half maximum for the O_2 1.27 μm, NO UV, and OH night airglows; hence $\beta=57$.

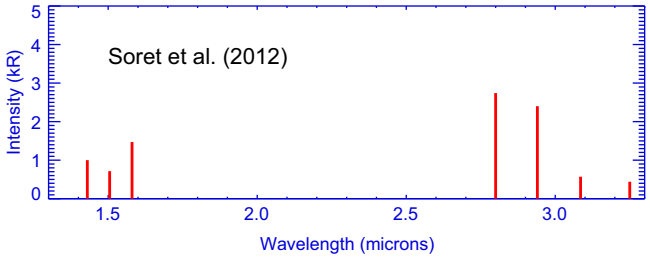

Fig. 1. Mean vertical intensities of the OH Δv=1 bands based on Soret et al. (2012). The OH Δv=2 band intensities are calculated by scaling of the Δv=1 bands to their transition probabilities. (2-0) 1.43 μm is the only band observed in the Δv=2 sequence near 1.5 μm.

Soret et al. (2012) averaged a few thousands observations of the OH nightglow and obtained a mean peak limb intensity of 350^{+350}_{-210} kR for the $\Delta v=1$ sequence. They identified the (1-0), (2-1), (3-2), and (4-3) bands in the $\Delta v=1$ sequence with a proportion of 44.6%, 39%, 9.3%, and 7.1%, respectively; hence their mean vertical intensities are 2.74, 2.4, 0.57, and 0.44 kR, respectively (Fig. 1). Then the (2-0), (3-1), and (4-2) bands in the $\Delta v=2$ sequence may be simply scaled using their transition probabilities (Fig. 1). However, this $\Delta v=2$ sequence disagrees with that observed, which consists of only the (2-0) band at 1.43 μm. Furthermore, the expected intensity of the (2-0) band is 16% of the $\Delta v=1$ sequence, while the observed ratio in Soret et al. (2012) is 38%. The $\Delta v=2$ sequence intensity, calculated by scaling of the Δv=1 bands and shown in Fig. 1, is 52% of that of $\Delta v=1$ Fig. 1.

Soret et al. (2012) understood these inconsistencies and focused at interpretation of the $\Delta v=1$ sequence neglecting the problems of the $\Delta v=2$ sequence. Here we accept this approach.

Table 3
Reactions, their rate coefficients, column rates, and mean altitudes.

#	Reaction	Rate coefficient[a]	Column rate[b]		*h* (km)	
1	$O+CO+M \rightarrow CO_2+M$	$2.2\times10^{-33}\ e^{-1750/T}$	6.44+6	5.10+6	94	95
2	$O+O+M \rightarrow O_2^*+M$[c]	$8.4\times10^{-25}\ T^{-3.25}$	7.76+11	7.46+11	101	101
3	$O+O_2+M \rightarrow O_3+M$	$1.2\times10^{-27}\ T^{-2.4}$	5.43+11	4.48+11	95	95
4	$O+O_3 \rightarrow O_2+O_2$	$8\times10^{-12}\ e^{-2060/T}$	5.53+7	8.59+7	96	97
5	$H+O_2+M \rightarrow HO_2+M$	$10^{-31}(300/T)^{1.3}$	1.33+11	4.67+11	95	93
6	$H+H+M \rightarrow H_2+M$	$6.6\times10^{-27}\ T^{-2.27}$	3.19+7	9.09+7	98	96
7	$H+O_3 \rightarrow OH^*+O_2$	$1.4\times10^{-10}\ e^{-470/T}$	1.29+11	4.31+11	96	95
8	$O+HO_2 \rightarrow OH^*+O_2$	$3\times10^{-11}\ e^{200/T}$	1.30+11	4.42+11	95	93
9	$O+OH \rightarrow O_2+H$	$1.8\times10^{-11}\ e^{180/T}$	2.47+11	7.27+11	96	95
10	$CO+OH \rightarrow CO_2+H$	$2.8\times10^{-13}\ e^{-176/T}$	1.29+10	1.84+11	94	92
11	$H+HO_2 \rightarrow OH+OH$	7.2×10^{-11}	6.95+8	1.98+10	95	92
12	$H+HO_2 \rightarrow H_2+O_2$	6.9×10^{-12}	6.67+7	1.90+9	95	92
13	$H+HO_2 \rightarrow H_2O+O$	1.6×10^{-12}	1.53+7	4.36+8	95	92
14	$OH+HO_2 \rightarrow H_2O+O_2$	$4.8\times10^{-11}\ e^{250/T}$	1.60+6	7.07+8	94	91
15	$HO_2+HO_2 \rightarrow H_2O_2+O_2$	$2.2\times10^{-13}\ e^{600/T}$	2.42+4	3.74+8	93	90
16	$OH+H_2 \rightarrow H_2O+H$	$2.8\times10^{-12}\ e^{-1800/T}$	2150	1.43+5	93	92
17	$OH+H_2O_2 \rightarrow HO_2+H_2O$	$2.9\times10^{-12}\ e^{-160/T}$	78	1.39+8	94	92
18	$OH+O_3 \rightarrow HO_2+O_2$	$1.7\times10^{-12}\ e^{-940/T}$	4.17+4	5.78+5	94	92
19	$HO_2+O_3 \rightarrow OH+2\ O_2$	$10^{-14}\ e^{-490/T}$	1432	2.93+5	93	88
20	$O+H_2O_2 \rightarrow OH+HO_2$	$1.4\times10^{-12}\ e^{-2000/T}$	110	1.19+7	96	97
21	$H+HCl \rightarrow H_2+Cl$	$6.6\times10^{-16}\ T^{1.44}\ e^{-1240/T}$	5.17+8	4.72+8	96	94
22	$OH+HCl \rightarrow H_2O+Cl$	$1.7\times10^{-12}\ e^{-230/T}$	2.33+8	1.31+9	94	92
23	$O+HCl \rightarrow OH+Cl$	$10^{-11}\ e^{-3300/T}$	2.34+6	7.11+5	95	96
24	$Cl+H_2 \rightarrow HCl+H$	$3.9\times10^{-11}\ e^{-2310/T}$	2.92+7	1.57+6	91	93
25	$Cl+HO_2 \rightarrow OH+ClO$	$1.8\times10^{-11}\ e^{170/T}$	2.72+9	1.71+9	94	91
26	$Cl+HO_2 \rightarrow OH+ClO$	$6.3\times10^{-11}\ e^{-570/T}$	1.08+8	7.39+7	94	91
27	$Cl+H_2O_2 \rightarrow HCl+HO_2$	$1.1\times10^{-11}\ e^{-980/T}$	2.35+4	6.67+7	93	93
28	$H+Cl_2 \rightarrow HCl+Cl$	$8\times10^{-11}\ e^{-416/T}$	6.74+9	3.15+6	93	93
29	$Cl+Cl+M \rightarrow Cl_2+M$	$5\times10^{-26}\ T^{-2.4}$	2.55+9	1.10+6	92	93
30	$H+Cl+M \rightarrow HCl+M$	10^{-32}	1.16+7	7.12+5	96	94
31	$Cl+O_3 \rightarrow ClO+O_2$	$2.8\times10^{-11}\ e^{-250/T}$	4.14+11	1.68+10	94	94
32	$ClO+O \rightarrow Cl+O_2$	$2.5\times10^{-11}\ e^{110/T}$	4.46+11	1.70+10	94	94
33	$Cl+CO+M \rightarrow ClCO+M$	$2.6\times10^{-34}\ e^{810/T}$	6.65+11	8.10+9	91	92
34	$ClCO+M \rightarrow Cl+CO+M$	$10^{-9}\ e^{-2960/T}$	4.35+11	3.68+9	90	91
35	$ClCO+Cl \rightarrow CO+Cl_2$	$1.1\times10^{-10}\ e^{-706/T}$	2.43+9	8.77+5	91	92
36	$ClCO+NO_2 \rightarrow CO_2+NO+Cl$	$6\times10^{-13}\ e^{600/T}$	7.55+7	3.97+4	89	88
37	$ClCO+O \rightarrow CO_2+Cl$	3×10^{-11}	1.91+11	4.10+9	93	93
38	$ClCO+O_2+M \rightarrow ClCO_3+M$	$5.7\times10^{-32}\ e^{500/T}$	3.65+10	3.17+8	90	91
39	$ClCO_3+Cl \rightarrow CO_2+Cl+ClO$	10^{-11}	2.60+10	8.28+6	89	90
40	$ClCO_3+O \rightarrow CO_2+Cl+O_2$	10^{-11}	1.06+10	2.67+8	91	91
41	$ClCO_3+H \rightarrow CO_2+Cl+OH$	10^{-11}	1.33+7	4.07+7	92	91
42	$N+O \rightarrow NO+h\nu$	$3.3\times10^{-16}\ T^{-0.5}$	4.25+8	4.25+8	111	111
43	$N+O+M \rightarrow NO+M$	$3.5\times10^{-31}\ T^{-0.5}$	1.08+8	1.05+8	98	98
44	$N+NO \rightarrow N2+O$	$2.1\times10^{-11}\ e^{100/T}$	6.37+8	6.39+8	105	105
45	$NO+O+M \rightarrow NO_2+M$	$10^{-27}\ T^{-1.5}$	1.28+7	9.79+6	97	98
46	$NO+O_3 \rightarrow NO_2+O_2$	$3\times10^{-12}\ e^{-1500/T}$	4384	7.19+6	93	81
47	$NO+HO_2 \rightarrow NO_2+OH$	$3.5\times10^{-12}\ e^{250/T}$	1.04+5	1.44+8	93	86
48	$NO_2+O \rightarrow NO+O_2$	$5.1\times10^{-12}\ e^{210/T}$	3.92+8	9.76+7	90	89
49	$NO_2+O+M \rightarrow NO_3+M$	$1.7\times10^{-26}\ T^{-1.8}$	5.16+5	2.75+5	90	85
50	$NO_3+NO \rightarrow 2\ NO_2$	$1.5\times10^{-11}\ e^{170/T}$	3.24+6	3.72+5	81	85
51	$NO_3+O \rightarrow NO_2+O_2$	10^{-11}	2.17+5	4.40+5	86	91
52	$N+O_2 \rightarrow NO+O$	$2\times10^{-18}\ T^{2.15}\ e^{-2560/T}$	4.52+5	6.74+5	93	92
53	$SO_2+O+M \rightarrow SO_3+M$	$5\times10^{-22}\ T^{-3}\ e^{-2400/T}$	2.34+6	1.67+6	94	94
54	$SO_2+OH+M \rightarrow HSO_3+M$	$3.5\times10^{-20}\ T^{-4.3}$	2.88+6	6.25+7	93	91
55	$SO_2+Cl+M \rightarrow ClSO_2+M$	$1.3\times10^{-34}\ e^{940/T}$	3.18+8	3.39+6	90	92
56	$ClSO_2+H \rightarrow SO_2+HCl$	10^{-11}	4.48+6	1.41+6	94	92
57	$ClSO_2+Cl \rightarrow SO_2+Cl_2$	10^{-12}	1.75+8	2.06+4	90	91
58	$ClSO_2+O \rightarrow SO_2+ClO$	10^{-12}	1.32+8	1.92+6	92	93
59	$HSO_3+O_2 \rightarrow SO_3+HO_2$	$1.3\times10^{-12}\ e^{-330/T}$	2.88+6	6.25+7	93	91
60	$O_2(^1\Delta)+M \rightarrow O_2+M$	10^{-20}	3.47+10	3.10+10	96	96
61	$O_2(^1\Delta) \rightarrow O_2+h\nu$	$2.24\times10^{-4}\ s^{-1}$	5.08+11	4.91+11	100	101
62[d]	$N+NO_2 \rightarrow NO+NO$	$5.8\times10^{-12}\ e^{220/T}$	8.28+7	8.17+7	83	89
63	$NO+ClO \rightarrow NO_2+Cl$	$6.2\times10^{-12}\ e^{295/T}$	5.70+8	3.93+7	89	87
64	$NO+Cl+M \rightarrow ClNO+M$	$2\times10^{-31}\ (300/T)^{1.8}$	3.54+6	1.71+4	91	90
65	$OH+ClO \rightarrow HCl+O_2$	$10^{-13}\ e^{600/T}$	2.16+5	5.16+5	93	91
66	$OH+ClO \rightarrow HO_2+Cl$	1.9×10^{-11}	1.10+7	2.78+7	93	91
67	$ClCO+ClNO \rightarrow COCl_2+NO$	$8\times10^{-11}\ e^{-573/T}$	243	0.7	90	90
68	$ClCO+Cl_2 \rightarrow COCl_2+Cl$	$4.2\times10^{-12}\ e^{-1490/T}$	4.57+5	0.06	90	91
69	$COCl_2+O \rightarrow ClCO+ClO$	10^{-14}	4.04+5	0.7	92	93
70	$ClNO+Cl \rightarrow NO+Cl_2$	$5.8\times10^{-11}\ e^{100/T}$	3.64+6	1.65+4	91	91
71	$ClNO+O \rightarrow NO+ClO$	$8.3\times10^{-12}\ e^{-1520/T}$	110	73	96	97
72	$NO+ClO_2 \rightarrow ClNO+O_2$	4.5×10^{-11}	1.01+5	525	91	93
73	$Cl+O_2+M \rightarrow ClO_2+M$	$5\times10^{-33}\ (300/T)^{3.1}$	4.91+11	5.73+9	91	92
74	$ClO_2+M \rightarrow Cl+O_2+M$	$7\times10^{-10}\ e^{-1820/T}$	4.90+11	5.73+9	91	92
75	$O+Cl_2 \rightarrow ClO+Cl$	$7.4\times10^{-12}\ e^{-1650/T}$	1.41+8	4074	92	94

Table 3 (*continued*)

#	Reaction	Rate coefficient[a]	Column rate[b]		*h* (km)	
76	$Cl+O+M \rightarrow ClO+M$	5×10^{-32}	8.75+9	1.64+8	97	96
77	$ClO_2+O \rightarrow ClO+O_2$	$2.4 \times 10^{-12}\ e^{-960/T}$	9.43+5	1.68+4	98	96
78	$ClO_2+Cl \rightarrow Cl_2+O_2$	2.3×10^{-10}	1.20+9	5.89+6	93	94
79	$ClO_2+Cl \rightarrow ClO+ClO$	1.2×10^{-11}	6.25+7	3.07+4	93	94
80	$ClSO_2+ClSO_2 \rightarrow SO_2Cl_2+SO_2$	10^{-12}	3.18+6	1.05+4	84	82
81	$NO_2+ClO+M \rightarrow ClNO_3+M$	$4 \times 10^{-31}\ (300/T)^{3.4}$	1.23+9	7.66+5	85	85
82	$ClNO_3+Cl \rightarrow Cl_2+NO_3$	$6.5 \times 10^{-12}\ e^{135/T}$	1.20+9	5.91+5	85	90
83	$ClO+ClO \rightarrow Cl_2+O_2$	$10^{-12}\ e^{-1590/T}$	1.28+8	51	85	88
84	$ClO+ClO \rightarrow ClO_2+Cl$	$3.5 \times 10^{-13}\ e^{-1370/T}$	1.50+8	62	85	88
85	$NO_3+Cl \rightarrow NO_2+ClO$	2.4×10^{-11}	3.87+8	5.31+4	87	90
86	$NO_3+ClO \rightarrow NO_2+ClO_2$	4.7×10^{-13}	8.05+8	818	84	88

[a] In $cm^3\ s^{-1}$ and $cm^6\ s^{-1}$ for two- and three-body reactions, respectively. References to the rate coefficients may be found in Table 5 in Krasnopolsky (2012). Rate coefficients of the reactions 80 to 86 are from Sander et al. (2011).

[b] For models A and B, in $cm^{-2}\ s^{-1}$ for column rates; 6.44+6=$6.44 \times 10^6\ cm^{-2}\ s^{-1}$.

[c] Yield of $O_2(^1\Delta)$ is 0.7; the rate coefficient from Smith and Robertson (2008) is increased by a factor of 2.5 to account for the higher efficiency of CO_2 than N_2 as a third body.

[d] Wennberg et al. (1994).

The OH (5-4) band at 3.43 μm is not seen in the published spectra in Piccioni et al. (2008) and Soret et al. (2012). The (5-3) band at 1.67 μm should be brighter than (5-4) by a factor of 12, and this band is not seen in Piccioni et al. (2008) as well. Therefore we will try to deplete production of $v=5$ in our model.

3. Photochemical model for the nighttime atmosphere

Reactions with H and Cl are the only effective loss processes for ozone in the nighttime atmosphere of Venus

$$H+O_3 \rightarrow OH^*+O_2$$

$$Cl+O_3 \rightarrow ClO+O_2.$$

To fit to the observed ozone layer, we will therefore increase the flux of H at the upper boundary and then involve a flux of Cl. Our study indicates that the reaction scheme in Kr10 is insufficient for large fluxes of H and Cl, and we added 25 reactions (r62–86 in Table 3) to our model. We changed a rate coefficient of the termolecular reaction of association of oxygen atoms (r2) that was recently measured by Smith and Robertson (2008) for N_2 as a third body. All rate coefficients of termolecular reactions are scaled in our model by a factor of 2.5 to account for the higher efficiency of CO_2 relative to N_2 as a third body (Krasnopolsky, 2012). Kr10 adopted a rate coefficient of the reaction between N and NO from Fox (1994) who adjusted it to fit observations in the martian atmosphere. Here we use its standard value from reviews of the laboratory data.

Temperature and eddy diffusion profiles in the model are shown in Fig. 2. The temperature profile is a combination of the VIRA profile below 100 km for latitude of 45° from Seiff et al. (1985) and the nighttime profile from Hedin et al. (1983) which is typically used in the Venus Express publications. The profile of eddy diffusion is similar to that in Kr10.

CO_2, HCl, and SO_2 are given by their densities at the lower boundary of 80 km. NO was observed (Krasnopolsky, 2006) with a mixing ratio of 5.5 ppb below 70 km and upward flux of $6 \times 10^7\ cm^{-2}\ s^{-1}$; this flux was adopted as a lower boundary condition in the model. The lower boundary conditions for all other species are flow velocities $V=-K/2H=-0.116$ cm s^{-1}, similar to those in Kr10. Here K is the eddy diffusion coefficient and H is the scale height. The upper boundary is closed (that is, fluxes are zero) for all species except CO, O, N, H, and Cl, and their fluxes are free parameters. Fluxes of CO, O, and N are similar to those in Kr10

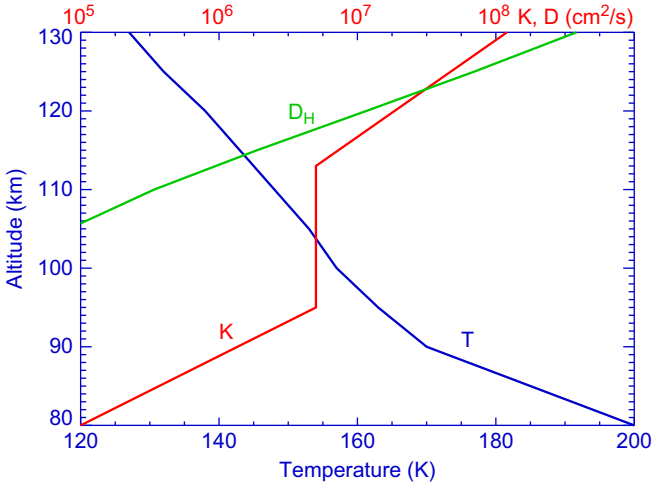

Fig. 2. Vertical profiles of temperature and eddy diffusion adopted in the model. Coefficient of molecular diffusion of H in CO_2 is shown for comparison.

and equal to 2×10^{12}, 3×10^{12}, and $1.2 \times 10^9\ cm^{-2}\ s^{-1}$, respectively, in our models.

The ozone profile from Kr10 is compared in Fig. 3 with those calculated in this model for the hydrogen fluxes $\Phi_H=10^8$, 10^9, and $10^{10}\ cm^{-2}\ s^{-1}$. The ozone profiles demonstrate a complicated behavior that looks irregular below the maximum near 93 km. The profile for $\Phi_H=10^{10}\ cm^{-2}\ s^{-1}$ approaches the observed peak value of $7 \times 10^7\ cm^{-3}$; however, the SPICAV stellar occultations revealed thin layers of ozone with FWHM of 5 to 10 km, while the calculated O_3 density grows to $4 \times 10^8\ cm^{-3}$ at 80 km. Our model for $\Phi_H=10^{10}\ cm^{-2}\ s^{-1}$ (model B) will be considered in Section 6.

To improve fitting to the ozone observations, we add a flux of Cl. Minor additions of Cl are ineffective, and the values comparable to that for H are required to fit the ozone observations. Our basic model A is for $\Phi_{Cl}=\Phi_H=10^{10}\ cm^{-2}\ s^{-1}$ (Fig. 3). It fits to the observed parameters of the ozone nighttime layer: peak density is $8 \times 10^7\ cm^{-3}$, peak altitude is 93.5 km, FWHM=6 km.

It is not clear a priori if the adopted fluxes of H and Cl are compatible with their abundances in the daytime mesosphere. Kr10 found that the required flux of O constitutes 45% of its production by photolysis of CO_2 above 80 km. The global-mean photochemical model (Krasnopolsky, 2012) is helpful to study the problem, and we found that the adopted fluxes are proportional to column densities of O, N, H, and Cl above 90 km in the model: Φ_O: Φ_N: Φ_H: Φ_{Cl}≈{O}: {N}: {H}: {Cl}. This is a convincing argument in

favor of the adopted fluxes. It looks like a lower boundary of the flow from the day side to the night side is near 90 km.

The calculated model is significantly different from that in Kr10. Its column reaction rates are given in Table 3, and the calculated vertical profiles of species are shown in Fig. 4. CO_2, CO, SO_2, and O_X (O, O_2, and O_3) are in the upper left panel. The calculated CO profile agrees with those in the nightside observations by Clancy et al. (2012).

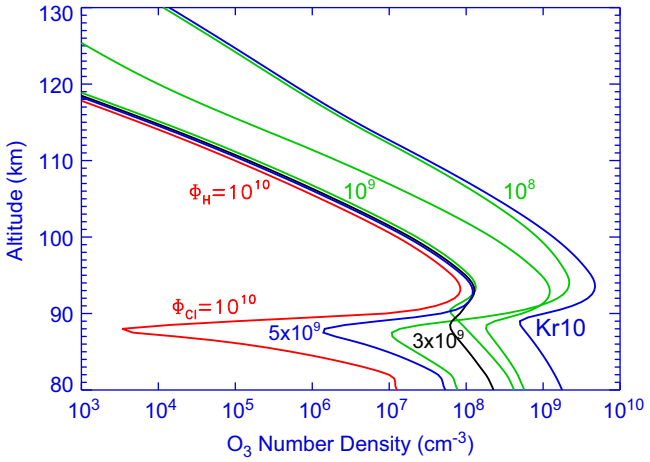

Fig. 3. Ozone profile as a function of fluxes of H and Cl in $cm^{-2}\ s^{-1}$ at the upper boundary. Green curves and the curve from Kr10 are for $\Phi_{Cl}=0$. The best fit to the observed O_3 (Montmessin et al., 2011) $\Phi_H=\Phi_{Cl}=10^{10}\ cm^{-2}\ s^{-1}$ (red). (For interpretation of the references to color in this figure legend, the reader is referred to the web version of this article.)

We will consider below stable forms of hydrogen (H_2O, HCl, and H_2), chlorine (HCl and Cl_2 at night), and nitrogen (N_2) and their radicals that are typically called as odd hydrogen, chlorine, and nitrogen in photochemical papers.

Major losses of odd hydrogen and odd chlorine are via reactions

$H+Cl_2 \rightarrow HCl+Cl$, $6.74\times10^9\ cm^{-2}\ s^{-1}$

$Cl+HO_2 \rightarrow HCl+O_2$, $2.72\times10^9\ cm^{-2}\ s^{-1}$.

Their sum is almost equal to $10^{10}\ cm^{-2}\ s^{-1}$, the adopted fluxes of H and Cl at the upper boundary. Odd hydrogen is partly transformed into odd chlorine via

$H+HCl \rightarrow H_2+Cl$, $5.17\times10^8\ cm^{-2}\ s^{-1}$

$OH+HCl \rightarrow H_2O+Cl$, $2.33\times10^8\ cm^{-2}\ s^{-1}$.

Therefore odd chlorine is more abundant than odd hydrogen below ≈95 km.

Atomic oxygen forms O_2 in the reactions

$O+O+M \rightarrow O_2^*+M$, $7.76\times10^{11}\ cm^{-2}\ s^{-1}$

$O+OH \rightarrow O_2+H$, $2.47\times10^{11}\ cm^{-2}\ s^{-1}$

$O+ClO \rightarrow O_2+Cl$, $4.46\times10^{11}\ cm^{-2}\ s^{-1}$.

The loss of O in these reactions is almost equal to the O flux at the upper boundary. The O flux at the upper boundary is converted into flux of O_2 at the lower boundary, and the O_2 mixing ratio at 80 km is $\Phi_O/(2Vn_{80})=8\times10^{-5}$. Therefore the O_2 profile and production of ozone (r3 $O+O_2+M$) do not depend on the adopted fluxes of H and Cl. Ozone is lost in $O_3+X \rightarrow XO+O_2$ followed by $O+XO \rightarrow O_2+X$; here X=H or Cl. These reactions

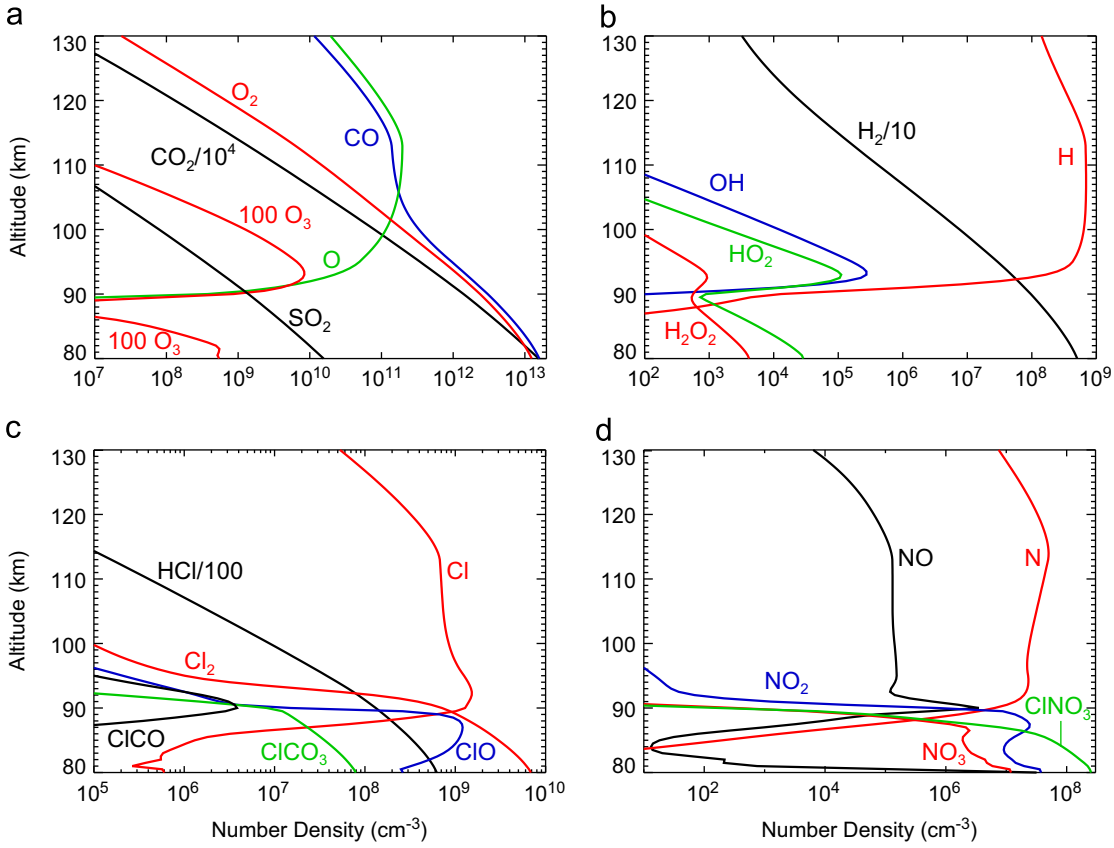

Fig. 4. Vertical profiles of species in the nighttime atmosphere of Venus (basic model): CO_2 products and SO_2 (a), hydrogen species (b), chlorine species (c), and odd nitrogen (d).

Table 4
Adopted fluxes at 130 km and some calculated fluxes and mixing ratios at 80 km in model A.

130 km:	O	CO	N	H	Cl	80 km	CO	O_2	H_2	Cl_2	ClO	NO	$ClNO_3$
Flux	3+12	2+12	1.2+9	1+10	1+10		1.9+12	1.5+12	6.1+8	8.2+8	3.1+7	6+7	3.0+7
Mixing Ratio							1.0–4	8.0–5	3.2–8	4.4–8	1.7–9	–	1.6–9

All fluxes are in $cm^{-2}\ s^{-1}$ and downward (except NO), fluxes at 80 km are corrected to the surface, i.e., multiplied by $(1+80/6052)^2 = 1.027$. Fluxes at 130 km have to be multiplied by $(1+130/6052)^2 = 1.043$ for correction to the surface. $3+12 = 3 \times 10^{12}$.

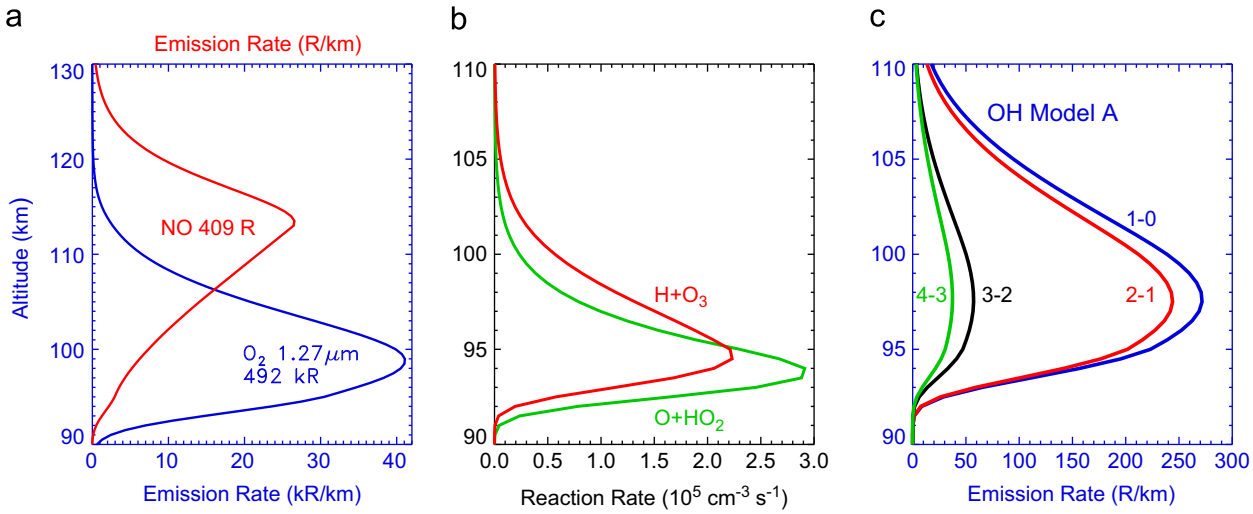

Fig. 5. Basic model: calculated vertical profiles of the O_2 1.27 μm and NO UV total ($\gamma+\delta$ bands) nightglow (a), two reactions of excitation of the OH nightglow (b), and four bands of the OH nightglow in the $\Delta v = 1$ sequence (c).

balance the production of ozone and also do not depend on the fluxes of H and Cl. That is why the rate of r2 O+O+M and the O_2 nightglow intensity do not depend on the fluxes of H and Cl at the upper boundary, although the reactions with odd hydrogen and chlorine remove half oxygen flux.

The calculated column abundances of Cl_2 and ClO (Fig. 4c) are rather high and equal to 3.6×10^{15} and $8 \times 10^{14}\ cm^{-2}$, respectively. All losses of Cl_2 and ClO (including their fluxes at 80 km, see Table 4) are equal to $7.7 \times 10^9\ cm^{-2}\ s^{-1}$ and $4.5 \times 10^{11}\ cm^{-2}\ s^{-1}$, respectively. Ratios of column abundances to column loss rates are chemical lifetimes that are equal to 5 days for Cl_2 and 30 min for ClO. Photolysis reduces the Cl_2 lifetime to 3 min on the day side. Duration of night is ~2 days at the cloud tops, and the expected Cl_2 nighttime column abundance is $\sim 7 \times 10^{14}\ cm^{-2}$. The Cl_2 cross section is $2.6 \times 10^{-19}\ cm^2$ at 330 nm (Sander et al., 2011), and its absorption is ~1.5% at 80 km in the occultation geometry. The Cl_2 absorption is continuous; therefore its detection against the aerosol extinction may be difficult.

The ClO mixing ratio reaches 48 ppb at 88 km; ClO has prominent absorption bands at 265–310 nm with a peak absorption cross section of $5.4 \times 10^{-18}\ cm^2$ at 280 nm (Sander et al., 2011). These bands could be seen in the UV stellar occultations. Odd nitrogen is also affected by chlorine chemistry (Fig. 4d), and the most abundant species at 80–85 km in Fig. 4d is $ClNO_3$. Its mixing ratio is 1.6 ppb at 80 km (Table 3). Absorption cross section of $ClNO_3$ gradually increases to $3 \times 10^{-18}\ cm^2$ at 216 nm (Sander et al., 2011), and the absorption is ~2.5% in the occultation mode.

The calculated vertical profile of the O_2 nightglow at 1.27 μm is shown in Fig. 5a. It is similar to that in Kr10, in spite of the increase in the flux of H by two orders of magnitude and the inclusion of the large flux of Cl. The calculated vertical intensity of 490 kR is close to 550 kR in Kr10. The NO nightglow profile is also similar to that in Kr10, and both O_2 and NO nightglow profiles agree with the mean nightside observations from Venus Express (Piccioni et al., 2009; Gerard et al., 2008, Fig. 5).

4. Excitation and quenching of the OH nightglow

There are two processes of excitation of the OH nightglow on the terrestrial planets

r7, $H+O_3 \rightarrow OH^*+O_2$

r8, $O+HO_2 \rightarrow OH^*+O_2$.

Kr10 suggested a scheme of excitation, quenching, and energy transfer in the OH nightglow on Venus that fitted the model data to the OH observations available at that time. However, densities of H and O_3 have changed in our model from those in Kr10 by orders of magnitude, new data on the OH nightglow band distribution and their intensities became available (Soret et al., 2012), and the problem should be revisited. The rate of $H+O_3$ exceeded that of $O+HO_2$ in Kr10 by a factor of 20 while they are almost equal in our model (Table 3, Fig. 5b).

Initial data for this revision are given in Table 5. They include yields of the OH vibrational states in $H+O_3$ from Garcia Munoz et al. (2005). Yields for $O+HO_2$ should reflect the conclusion by Kaye (1988) that little or no population of $v \geq 4$ is expected from this process. We increase quenching rate coefficients of OH(v) by CO_2 from Garcia Munoz et al. (2005) by a factor of $300/T \approx 1.6$ (Table 5). This increase was recommended by Soret et al. (2012) with a reference to an abstract by Romanescu et al. (2009). (Actually that abstract does not contain any numerical data, and Soret et al. applied a factor of 2.3.) Mean rotational temperature of the O_2 nightglow at 1.27 μm is $T = 187 \pm 3$ K (Kr10) from observations by five independent teams, and the correction factor is 300/

Table 5
Fractional yields γ of OH(v') in the two excitation processes, rate coefficients of quenching by CO_2, and total transition probabilities of vibrational states of OH.

v'	γ_{H+O_3}	γ_{O+HO_2}	k_{CO_2} ($cm^3\ s^{-1}$)	A(v') (s^{-1})
0	0	0/0.2	–	–
1	0	0/0.2	2.9×10^{-13}	22.74
2	0	0/0.25	6.9×10^{-13}	45.85
3	0	0/0.25	2.2×10^{-12}	70.48
4	0.05	0/0.1	4.5×10^{-12}	97.56
5	0.05	0	1.25×10^{-11}	127.7
6	0.07	0	3.2×10^{-11}	161.3
7	0.19	0	1.1×10^{-10}	198.4
8	0.29	0	1.0×10^{-10}	237.8
9	0.35	0	9.1×10^{-11}	275.9

γ_{H+O_3} and A(v') are from Garcia Munoz et al. (2005), k_{CO_2} are from Garcia Munoz et al. (2005) and scaled by a factor of 300/T=1.6, and the adopted values of γ_{O+HO_2} for model A1; $\gamma_{O+HO_2}=0$ for all v' in models A and B.

Table 6
Calculated band intensities of the $\Delta v=1$ sequence (in kR) in various models and those observed by Soret et al. (2012).

Model	(1-0)	(2-1)	(3-2)	(4-3)	sum	(1-0)/(4-3)
Observed	2.74	2.40	0.57	0.44	6.15	6.3
$v''=0$, $\gamma=0$	0.005	0.007	0.002	0.020	0.034	0.25
$v''=0$, $\gamma=0.25$	0.97	0.51	0.17	0.020	1.67	48
$\delta v=1$, $\gamma=0$	5.61	3.07	1.05	0.38	10.1	15
$\delta v=1$, $\gamma=0.25$	8.32	4.06	1.21	0.38	14.0	22
$\delta v=1,2$; $\gamma=0$	3.91	2.12	0.71	0.26	7.00	15
$\delta v=1,2$; $\gamma=0.25$	5.98	2.86	0.88	0.26	10.0	23
equal $v''\leq 4$, $\gamma=0$	2.95	1.08	0.27	0.09	4.39	33
equal $v''\leq 4$, $\gamma=0.25$	4.79	1.74	0.44	0.09	7.06	53
Model A (Table 7)	2.73	2.40	0.57	0.39	6.09	7.0
Model A1 (Table 7)	2.75	2.40	0.57	0.41	6.13	6.7

γ is the adopted yield of OH($v'=0$ to 3) in $O+HO_2$.

187=1.6. We also use the OH transition probabilities from Garcia Munoz et al. (2005), and their sums for each v are given in Table 5. Densities of O are much smaller than those of CO_2 within the OH nightglow layer (90–110 km); therefore quenching of OH (v) by O is much weaker that that by CO_2 and may be safely neglected.

Vibrational states v'' of the quenching products in

$$OH(v')+CO_2\rightarrow OH(v'')+CO_2$$

are unknown, and two extreme cases are typically considered: sudden death with $v''=0$ and collisional cascade with $\delta v=v'-v''=1$. We have tested a few hypotheses for our basic model A (Table 6). Sudden death with no yield ($\gamma=0$) from $O+HO_2$ gives intensities that are smaller than observed by a factor of 200. If $\gamma=0.25$ for $v'=$ 0 to 3 in $O+HO_2$, then the intensity is 0.27 of that observed and the band distribution is very different from that observed. The next cases are the collisional cascade with $\gamma=0$ and 0.25. The total intensity and the (1-0)/(4-3) ratio significantly exceed the observed values for both cases (Table 6).

Then we calculated modifications to the collisional cascade when both $\delta v=1$ and 2 are equally probable. We considered also cases when each quenching of OH($v'>4$) populates equally $v''=0$ to 4, $v'=4$ populates equally $v''=0$ to 3, etc. All these versions of the excitation transfer do not fit the observed band intensities and relative distribution.

Two versions in Table 6 agree with the Venus Express observations of the $\Delta v=1$ sequence (Soret et al., 2012). R8 $O+HO_2$ does not excite OH in model A while the yields are equal to those in Table 5 in model A1. Both models involve the collisional cascade $\delta v=1$ for $v'=9$, 8, 7, and 5; $v'=6$ cascades to $v''=4$, and yields of v'' for $v'=4$ to 2 are given in Table 7. The calculated vertical profiles of the OH bands of the $\Delta v=1$ sequence in model A are shown in Fig. 5c. Peak altitudes for volume emission rates are at 98 km. Peak airglow altitudes for the limb observations are typically lower by ~2 km and agree with the Venus Express observations (Soret et al., 2012). Peak altitudes are lower in model A1 by 1.7 km; therefore model A without excitation of OH by $O+HO_2$ is preferable. The calculated (5-3) band at 1.67 μm (Section 2) is 0.04 kR and too weak to be observed, in accord with the published spectra (Piccioni et al., 2008; Soret et al., 2012).

5. Variations of night airglow and ozone

The calculated model is aimed to reflect the mean nightside conditions. However, the night airglow on Venus is a very variable phenomenon. Delivery of O, N, H, and Cl from the day side to the night side is a complicated dynamical process and a basic though not only source of the nightglow variations. Photochemical response of the atmosphere to this delivery may be studied using our model with variable fluxes at the upper boundary. That was made in Kr10, and here we do the same with our updated model.

The O_2 nightglow at 1.27 μm is insensitive to variations of fluxes of N, H, and Cl, and its vertical intensity is

$$4\pi I_{O_2}=127(\Phi_O/10^{12})^{1.22}kR.$$

The power index exceeds one; therefore a partition between the loss of O in the termolecular association and those by odd hydrogen and chlorine chemistries is shifted to the former at high fluxes of O. The O_2 nightglow quantum yield is $0.5\times0.5\times0.7=0.17$ per oxygen atom. Here half O atoms are involved in the O_2 association, the next 0.5 is because two atoms are lost in the O_2 association, and 0.7 is the yield of $O_2(a^1\Delta_g)$.

Vertical intensity of the total NO UV nightglow (γ and δ band systems) is

$$4\pi I_{NO}=225(\Phi_N/10^9)(\Phi_O/10^{12})^{0.35}R.$$

The NO nightglow mean quantum yield is 0.34 per nitrogen atom. Both N and O atoms participate in the NO excitation; however, atomic oxygen is much more abundant than atomic nitrogen, and the nightglow dependence on the O flux is rather weak. Alternative losses of atomic nitrogen are in r43 N+O+M, r44 N+NO, and r62 $N+NO_2$.

The OH nightglow demonstrates a complicated dependence on the fluxes of O, H, and Cl. Vertical intensity of the $\Delta v=1$ band sequence is

$$4\pi I_{OH}=1.2\,(\Phi_O/10^{12})^{1.4}\,\frac{X^{1.47-0.46\ln X}}{Y^{1.43+0.65\ln Y}}\,kR;X=\frac{\Phi_H}{10^{10}},Y=\frac{\Phi_{Cl}}{10^{10}}.$$

Excitation of the OH nightglow involves a few processes, and the term of quantum yield is inadequate for their description. If the logarithmic terms are neglected, then the intensity is proportional to $(\Phi_O\Phi_H/\Phi_{Cl})^{1.4}$. High correlation between the OH and $O_2(a^1\Delta_g)$ nightglows (Gerard et al., 2012) is explained by the almost equal power indices for Φ_O in the relationships for their intensities.

Variations of the nighttime peak ozone number density may be of some interest as well:

$$[O_3]_{max}=\frac{2.2\times10^7(\Phi_O/10^{12})^{1.2}}{Y^{0.74+0.3\ln Y}}\,cm^{-3}.$$

The observed variations of the peak ozone density are from 2×10^7 to 10^8 cm^{-3} (Montmessin et al., 2011) and well covered by this formula. The calculated altitude of the ozone peak varies from 92 to 95 km, and this range is smaller than that observed.

Table 7
Adopted yields of OH(v'') in quenching of OH(v') by CO_2 for models A, A1, and B (given as A/A1/B).

$V''\backslash V'$	2	3	4	5	6	7	8	9
0	0.59/0.8/0.4	0.2/0.5/0	0/0.2/0.75	0/0/0	0/0/0.4	0/0/0	0/0/0	0/0/0
1	0.41/0.2/0.6	0.25/0.1/0	0/0.1/0	0/0/0	0/0/0	0/0/0	0/0/0	0/0/0
2	–	0.55/0.4/1	0.46/0.35/0	0/0/0	0/0/0.1	0/0/0	0/0/0	0/0/0
3	–	–	0.54/0.35/0.25	0/0/0	0/0/0.1	0/0/0	0/0/0	0/0/0
4	–	–	–	1/1/1	1/1/0.4	0/0/0	0/0/0	0/0/0
5	–	–	–	–	0/0/0	0/0/0	0/0/0	0/0/0
6	–	–	–	–	–	1/1/1	0/0/0	0/0/0
7	–	–	–	–	–	–	1/1/1	0/0/0
8	–	–	–	–	–	–	–	1/1/1

6. Model without chlorine flux at 130 km

This model with $\Phi_H = 10^{10}$ cm^{-2} s^{-1} and no chlorine flux (Section 3 and Fig. 3) resulted in the ozone profile with the peak density and altitude that are close to those observed by the SPICAV stellar occultations (Montmessin et al., 2011). However, the calculated ozone density increases to 4×10^8 cm^{-3} at 80 km, and there are no indications to this increase in the observations. On the other hand, the aerosol extinction becomes significant in the SPICAV occultation below 90 km and makes the retrieved ozone densities uncertain at these altitudes. Therefore the calculated ozone for the model without the chlorine flux at 130 km is not ruled out by the observations, and we will consider this model (model B) in more detail.

Vertical profiles of species calculated for model B are shown in Fig. 6 and may be compared with those in model A in Fig. 4. The main photochemical products of CO_2 are CO, O_2, and O, and their profiles are similar in both models. The ozone densities are larger in model B below 90 km, because its loss in the reaction with Cl becomes ineffective.

The hydrogen flux from the upper boundary is lost in recombination of odd hydrogen:

R12	$H+HO_2 \rightarrow H_2+O_2$	1.90×10^9 cm^{-2} s^{-1}
R13	$H+HO_2 \rightarrow H_2O+O$	4.36×10^8 cm^{-2} s^{-1}
R14	$OH+HO_2 \rightarrow H_2O+O_2$	7.07×10^8 cm^{-2} s^{-1}
R17	$OH+H_2O_2 \rightarrow H_2O+HO_2$	1.39×10^8 cm^{-2} s^{-1}
Total		3.18×10^9 cm^{-2} s^{-1}

and in reactions

R21	$H+HCl \rightarrow H_2+Cl$	4.72×10^8 cm^{-2} s^{-1}
R22	$OH+HCl \rightarrow H_2O+Cl$	1.31×10^9 cm^{-2} s^{-1}
R25	$Cl+HO_2 \rightarrow HCl+O_2$	1.71×10^9 cm^{-2} s^{-1}
Total		3.49×10^9 cm^{-2} s^{-1}.

The loss of odd hydrogen in these reactions is $2 \times 3.18 \times 10^9 + 3.49 \times 10^9 = 9.85 \times 10^9$ cm^{-2} s^{-1} and equals the supply of H.

The above reactions r21 and r22 are main sources of odd chlorine in model B, and r25 is its major loss. Although an external supply of atomic chlorine is lacking in the model, its ambient production is significant and equal to 18% of the flux in model A.

Peroxide H_2O_2 is much more abundant in model B (Fig. 6b) than in model A. Its production of 3.8×10^8 cm^{-2} s^{-1} in r15 HO_2+HO_2 may be compared to its column abundance of 8.3×10^{14} cm^{-2} to give chemical lifetime of 2.2×10^6 s, that is, 25 days. It is much longer that the duration of night in the middle atmosphere, and typical nighttime densities of H_2O_2 are smaller than those in Fig. 6b by a factor of ~20. These densities are too low for detection by the UV stellar occultation spectroscopy or high-resolution spectroscopy at 8 μm. Photolysis on the day side quickly removes peroxide to a negligible level. NO_2 is another abundant species; its lifetime is 4 days, and typical nighttime densities are smaller that than shown in Fig. 6d by a factor of 4. The estimated NO_2 cannot be detected by the occultation and infrared spectroscopy.

The calculated O_2 and NO nightglows (Fig. 7a) are similar to those in model A (Fig. 5a). Reactions r7 $H+O_3$ and r8 $O+HO_2$ (Fig. 7b) that may excite the OH nightglow are stronger than those in model A by a factor of 3.3. Column rates of r7 and r8 are similar, and the reactions peak at 94 and 92.5 km, respectively. The latter is lower that the observed OH nightglow that peaks at 96 km on the limb (Soret et al., 2012), and we neglect production of OH(v) in r8, that is, $\gamma_{O+HO2} = 0$ in model B. Chosen yields of OH(v'') in quenching of OH(v') by CO_2 that fit the observed $\Delta v = 1$ band distribution are given in Table 7. Calculated vertical profiles of volume emission rates for the four $\Delta v = 1$ bands are shown in Fig. 7c. The peak limb intensity is expected at 94 km, slightly lower than that observed. Ozone densities at 80 km are equal to ~10^7 cm^{-3} and 4×10^8 cm^{-3} in models A and B, respectively, and their observations are a basic tool to choose between the models.

Analytic expressions for the vertical intensities of the O_2 and NO nightglows are similar to those in model A. A relationship for vertical intensity of the OH $\Delta v = 1$ band sequence at 2.9 μm is

$$4\pi I_{OH}(kR) = 1.12 \frac{(\Phi_O/10^{12})^{1.55}}{(\Phi_H/10^{10})^{0.1}}.$$

The peak ozone density near 93 km is

$$[O_3]_{max} = 5.3 \times 10^7 \frac{\Phi_O/10^{12} - 0.5}{(\Phi_H/10^{10})^{1.1}} \text{cm}^{-3}.$$

The ozone density at 80 km is

$$[O_3]_{80km} = 10^8 \frac{8.5 - 11.2X + 7X^2}{(\Phi_H/10^{10})^{0.8}} \text{ cm}^{-3}; X = \ln(\Phi_O/10^{12}).$$

7. CO_2 densities in the Venus mesosphere

Soret et al. (2012) calculated the OH nightglow using the sudden death and collisional cascade $\delta v = 1$ (single quantum) quenching with adopted vertical profiles of O, O_3, H, and CO_2. The OH(v) excitation in $O+HO_2$ was neglected, and atomic oxygen was involved as a quencher of OH(v), although its effect is actually very low. The H profile from Kr10 was scaled to a peak value of 10^8 cm^{-3}. A CO_2 profile was a mean from the SPICAV stellar occultations. The sudden death model gave very low intensities while the OH nightglow intensities are too high in the single quantum model. Therefore the mean ozone profile from the SPICAV stellar occultations was reduced by a factor of 10 to fit the observed OH nightglow. The calculated band distribution is

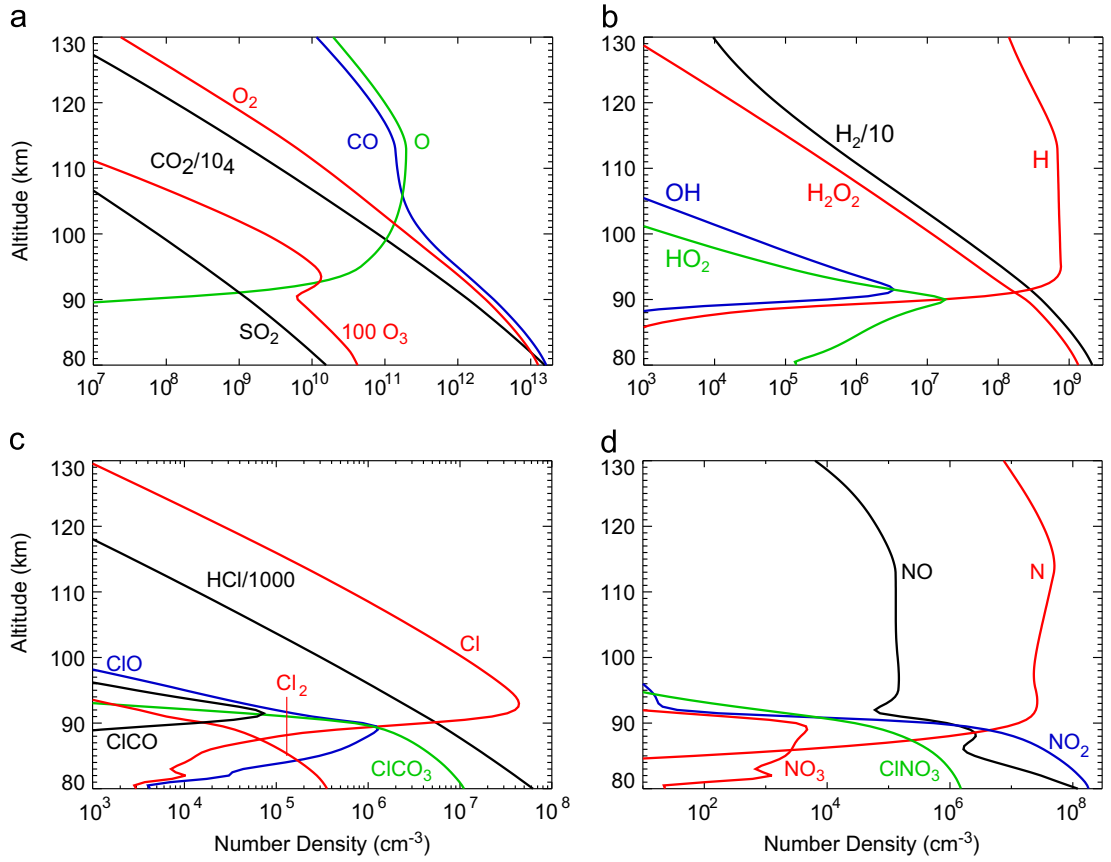

Fig. 6. Model without flux of chlorine at 130 km (model B). Vertical profiles of species in the nighttime atmosphere of Venus: CO_2 products and SO_2 (a), hydrogen species (b), chlorine species (c), and odd nitrogen (d).

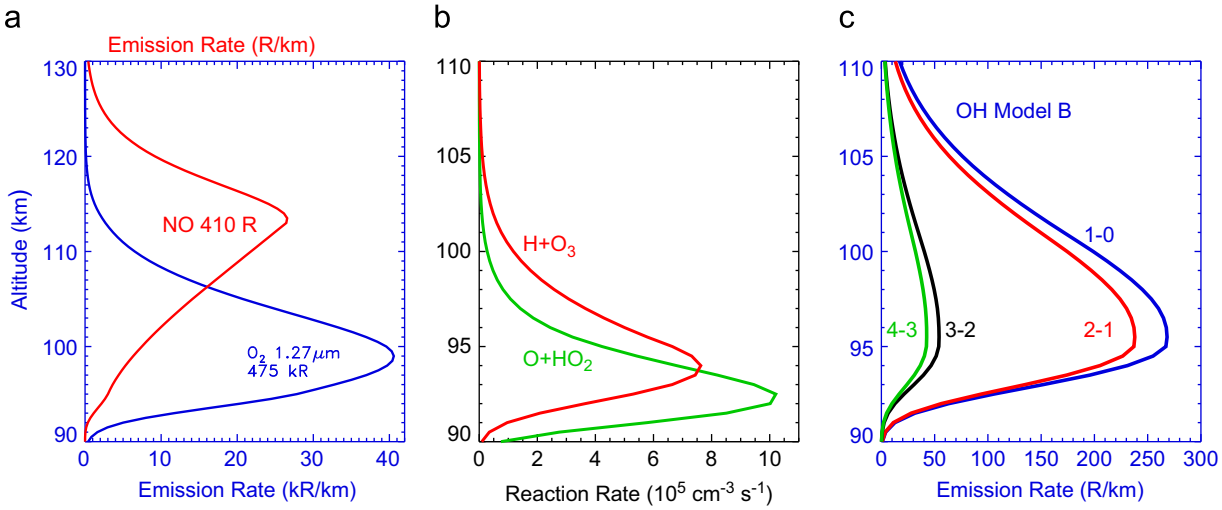

Fig. 7. Model without flux of chlorine at 130 km (model B): Calculated vertical profiles of the O_2 1.27 μm and NO UV total ($\gamma+\delta$ bands) nightglow (a), two reactions of excitation of the OH nightglow (b), and four bands of the OH nightglow in the $\Delta v=1$ sequence (c).

similar to those for the collisional cascade models in fig. 8 of Garcia Munoz et al. (2005) and in our Table 6.

Mean CO_2 densities at 100 and 80 km from the SPICAV stellar occultations (Soret et al., 2012) are compared with those from the Venus reference atmospheres in Table 8. Mean values for latitude of 45° are taken from Seiff et al. (1985), and nighttime data from the other references are given; the results are corrected for 3.4% of N_2. While differences between the reference atmospheres are of a few percent, the SPICAV data are smaller than those from the reference atmospheres at 100 and 80 km by factors of 2.5 and 10, respectively. The reference atmospheres between 100 and 80 km are based on the accelerometer data from the entry probes, radio occultations from the orbiters, and inversions of the CO_2 thermal emission at 15 μm and 4.3 μm. While individual points demonstrate some scatter, the mean data from all three methods are rather consistent and do not support the values from Soret et al. (2012) as well as a warm nighttime layer near 100 km (Bertaux et al., 2007) from the SPICAV stellar occultations. The Venus

Table 8
Nighttime densities of CO_2 (in cm^{-3}) at 100 and 80 km from SPICAV stellar occultations (Soret et al., 2012) and in the Venus reference atmospheres.

h (km)	Soret et al. (2012)	Hedin et al. (1983)	Keating et al. (1985)	Seiff et al. (1985)	Zasova et al. (2006)
100	4.2+14	1.03+15	1.07+15	1.10+15	1.03+15
80	1.3+16	–	–	1.48+17	1.34+17

4.2+14=4.2×10^{14}.

Express radio occultations (Tellmann et al., 2012) and observations at 4.3 μm (Migliorini et al., 2012) as well as general circulation models for the Venus thermosphere (Bougher et al., 1990; Brecht et al., 2011) typically agree with the reference atmospheres. Attempts to simulate the warm nighttime layer at 100 km by general circulation models were unsuccessful. All high-resolution observations of the O_2 nightglow at 1.27 μm resulted in rotational temperatures $T \approx 187$ K near 95 km (Kr10) and disagree with the warm nighttime layer with temperature increasing from 180 K near the terminator to 250 K at the antisolar point. Comparison of $[CO_2] = 1.2 \times 10^{16}$ cm^{-3} at 80 km from Soret et al. (2012) with $[CO_2] = 2.8 \times 10^{18}$ cm^{-3} and $T = 238$ K measured directly at 65 km by the Pioneer Venus night probe results in extremely low temperatures between these altitudes that are impossible in the Venus mesosphere. The CO_2 densities from the SPICAV stellar occultations were applied in analyses of the Venus nightglow by Soret et al. (2012) and Gerard et al. (in press) and adversely affect their conclusions.

8. Comparison with other models

Daytime odd nitrogen chemistry for the solar maximum conditions in the Venus thermosphere was studied by Fox (1982), Krasnopolsky (1983b), and Gerard et al. (1988). Those one-dimensional models were aimed to simulate observations of N by the Pioneer Venus orbiter neutral mass spectrometer. Odd nitrogen chemistry is initiated by production of N in predissociation of N_2 at 80–100 nm, electron impact dissociation of N_2, dissociative ionization of N_2 by photons and photoelectrons, and some ion reactions. Atomic nitrogen is formed in the ground state $N(^4S)$ and in the metastable state $N(^2D)$ in almost equal proportion. $N(^2D)$ is quenched to $N(^4S)$ by O and CO and reacts with CO_2 to form NO. Odd nitrogen is lost in the reaction $N+NO \rightarrow N_2+O$. There is some excess of N over NO on Venus, and this excess is transported either to the mesosphere by eddy diffusion or to the night side by winds across the terminator. The latter excites the NO UV nightglow.

One-dimensional models do not account for the horizontal transport in the atmosphere. Observations of the NO nightglow by the Pioneer Venus ultraviolet spectrometer at high solar activity and the recent observations by SPICAV at low solar activity were simulated by three-dimensional models by Bougher et al. (1990) and Brecht et al. (2011). Bougher et al. (1990) applied their basic model to the low solar activity as well.

Krasnopolsky (1983b) calculated the dayside production of N in both states at 1.1×10^{10} cm^{-2} s^{-1} at solar maximum and zenith angle of 60° (mean dayside conditions). This production was equal to 1.3×10^{10} cm^{-2} s^{-1} in Gerard et al. (1988) and 9.4×10^{9} cm^{-2} s^{-1} in Bougher et al. (1990) at solar maximum. The production at solar minimum was 4.5×10^{9} cm^{-2} s^{-1} in Bougher et al. (1990) and 1.58×10^{10} cm^{-2} s^{-1} in Brecht et al. (2011). All these values are in mutual agreement except that from Brecht et al. (2011) which exceeds the production in Bougher et al. (1990) by a factor of 3.5.

Krasnopolsky (1983b) calculated a net excess of N over NO at 3.2×10^{9} cm^{-2} s^{-1} at solar maximum and argued that the most of this excess is transported to the night side. The net delivery of N to the night side in Bougher et al. (1990) was equal to 1.9×10^{9} cm^{-2} s^{-1} and 5.8×10^{8} cm^{-2} s^{-1} at solar maximum and minimum, respectively. The nightglow effective yield is 0.34 in Kr10 and our current model. Using this yield, the values from Bougher et al. (1990) are converted to the mean nightside intensities of 650 and 200 R at solar maximum and minimum, respectively. The mean nightside NO airglow is 680 R at solar minimum in Brecht et al. (2011). The mean flux of N of 1.2×10^{9} cm^{-2} s^{-1} and the mean NO nightglow of 400 R at solar minimum in our model are between the values from Bougher et al. (1990) and Brecht et al. (2011).

Bougher and Borucki (1994) retrieved the visible O_2 nightglow intensities from the Pioneer Venus star tracker observations and applied their three-dimensional model to simulate variations of the O_2 visible nightglow and that at 1.27 μm. They included fixed profiles of some odd hydrogen and chlorine species from model C by Yung and DeMore (1982) in their model. An effective yield of $O_2(a^1\Delta_g)$ in the termolecular association was adopted at 0.27, and their basic model resulted in the O_2 nightglow at 1.27 μm with a peak of 0.54 MR near the antisolar point. The intensity was smaller by a factor of 2 at ~45° from the antisolar point and then to ~0.03 MR near the terminator. Scaling to the $O_2(a^1\Delta_g)$ yield of 0.7 (Krasnopolsky, 2011), the anitisolar maximum is 1.4 MR, similar to that of 1.2 MR observed by Venus Express (Piccioni et al., 2009).

The 3D model by Brecht et al. (2011) involves fixed profiles of some odd hydrogen and chlorine species from Kr10 and results in the O_2 nightglow at 1.27 μm with a peak intensity of 1.76 MR near the antisolar point and a mean intensity of 0.51 MR in a box of 60°S to 60°N and local times from 20:00 to 4:00, in reasonable agreement with the observations. The dayside net production of atomic oxygen is 2.34×10^{12} cm^{-2} s^{-1}, comparable with the flux of 3×10^{12} cm^{-2} s^{-1} in our model.

Analyzing laboratory data and observations of all oxygen band systems in the nightglows on the terrestrial planets, Krasnopolsky (2011) adopted theoretical yields of seven O_2 states in the termolecular association. He concluded that if quenching of a weakly bound $O_2(^5\Pi_g)$ state by CO_2 results in 90% of the singlet states and 10% of the triplet states, then the effective yield of $O_2(a^1\Delta_g)$ is 0.7. The yield is 0.75 if the triplet states of O_2 do not appear in this process. Generally there are no reasons to rule out the triplet states, and the value of 0.75 may be considered as an upper limit while 0.7 is a more probable value. All VEX papers applied the yield of 0.75 with a reference to Crisp et al. (1996), who actually estimated the yield of $O_2(a^1\Delta_g)$ at ~0.6–0.75.

9. Conclusions

Interpretation of detailed observations of the Venus night airglow by Venus Express requires adequate models for this phenomenon. The nightglow is initiated by atomic species that are transported from the day side, and three-dimensional models are needed to properly reproduce the atmospheric dynamics. However, chemistry is insufficient and incomplete in those models, and one-dimensional models complement them. Here we suggest a revision of the photochemical model for the Venus nighttime atmosphere and night airglow by Krasnopolsky (2010). This revision accounts for the detection of the nighttime ozone layer (Montmessin et al., 2011) and more detailed spectroscopy and morphology of the OH nightglow (Soret et al., 2012). Nighttime chemistry on Venus is induced by fluxes of O, N, H, and Cl with mean hemispheric values of 3×10^{12}, 1.2×10^{9}, 10^{10}, and 10^{10} cm^{-2} s^{-1}, respectively. These fluxes are proportional to column abundances of these species in the daytime atmosphere

above 90 km, and this favors their validity. The model includes 86 reactions of 29 species. The calculated abundances of Cl_2, ClO, and $ClNO_3$ exceed a ppb level at 80–90 km, and possibilities of their detection are briefly discussed. Properties of the ozone layer in the model agree with those observed by SPICAV. An alternative model without the flux of Cl agrees with the observed O_3 peak altitude and density but predicts an increase of ozone to 4×10^8 cm^{-3} at 80 km. Reaction rates of $H+O_3$ and $O+HO_2$ are equal; however, the latter is shifted to 92–94 km, and the models agree better with the observations if $O+HO_2$ does not contribute to excitation of the OH nightglow. Schemes for quenching of the OH vibrational quanta by CO_2 are chosen to fit the observed band distribution in the $\Delta v=1$ sequence at 2.9 μm. The model agrees with all observational constraints for the mean nighttime atmosphere. Analytic relationships between the nightglow intensities, the ozone layer, and the input fluxes of atomic species are given. The model results are compared with those of three-dimensional models for the Venus thermosphere.

Acknowledgment

This work is supported by a grant of the Russian Government to the Moscow Institute of Physics and Technology and to V.A. Krasnopolsky.

References

Bertaux, J.L., et al., 2007. A warm layer in Venus' cryosphere and high-altitude measurements of HF, HCl, H_2O and HDO. Nature 450, 646–649.
Bougher, S.W., Gerard, J.C., Stewart, A.I.F., Fesen, C.G., 1990. The Venus nitric oxide airglow: model calculations based on the Venus thermosphere general circulation model. Journal of Geophysical Research 95, 6271–6284.
Bougher, S.W., Borucki, W.J., 1994. Venus O_2 visible and IR nightglow: implications for lower thermosphere dynamics and chemistry. Journal of Geophysical Research 99, 3759–3776.
Brecht, A.S., Bougher, S.W., Gérard, J.-C., Parkinson, C., Rafkin, S., Foster, B., 2011. Understanding the variability of nightside temperatures, NO UV and O_2 IR nightglow emissions in the Venus upper atmosphere. Journal of Geophysical Research 116, E08004, http://dx.doi.org/10.1029/2010JE003770.
Clancy, R.T., Sandor, B.J., Moriarty-Schieven, G., 2012. Thermal structure and CO distribution for the Venus mesosphere/lower thermosphere: 2001–2009 inferior conjunction sub-millimeter CO absorption line observations. Icarus 217, 779–793.
Connes, P., Noxon, J.F., Traub, W.A., Carleton, N.P., 1979. $O_2(^1\Delta)$ emission in the day and night airglow of Venus. Astrophysical Journal 233, L29–L32.
Crisp, D., Meadows, V.S., Bezard, B., de Bergh, C., Maillard, J.P., Mills, F.P., 1996. Ground-based near-infrared observations of the Venus nightside: 1.27-μm $O_2(a^1\Delta_g)$ airglow from the upper atmosphere. Journal of Geophysical Research 101, 4577–4594.
Feldman, P.D., Moos, H.W., Clarke, J.T., Lane, A.L., 1979. Identification of the UV nightglow from Venus. Nature 279, 221–223.
Fox, J.L., 1982. The chemistry of metastable species in the Venusian atmosphere. Icarus 51, 248–260.
Fox, J.L., 1994. Rate coefficient for the reaction N+NO. Journal of Geophysical Research 99, 6273–6276.
Fox, J.L., 2012. The ionospheric source of the red and green lines of atomic oxygen in the Venus nightglow. Icarus 221, 787–799.
Garcia Munoz, A., McConnell, J.C., McDade, I.C., Melo, S.M.L., 2005. Airglow on Mars: some model expectations for the OH Meinel bands and the O_2 IR atmospheric band. Icarus 176, 75–95.
Garcia Munoz, A., Mills, F.P., Piccioni, G., Drossart, P., 2009a. The near-infrared nitric oxide nightglow in the upper atmosphere of Venus. Proceedings of the National Academy of Sciences 106, 985–988.
Garcia Munoz, A., Mills, F.P., Slanger, T.G., Piccioni, G., Drossart, P., 2009b. Visible and near-infrared nightglow of molecular oxygen in the atmosphere of Venus. Journal of Geophysical Research 114, E12002.
Gerard, J.C., Deneye, E.J., Lerho, M., 1988. Sources and distribution of odd nitrogen in the Venus daytime thermosphere. Icarus 75, 171–184.
Gerard, J.C., Cox, C., Saglam, A., Bertaux, J.L., Villard, E., Nehme, C., 2008. Limb observations of the ultraviolet nitric oxide nightglow with SPICAV on board Venus Express. Journal of Geophysical Research 113, E00B03.
Gerard, J.C., Soret, L., Piccioni, G., Drossart, P., 2012. Spatial correlation of OH Meinel and O_2 infrared atmospheric nightglow emissions observed with VIRTIS-M on board Venus Express. Icarus 217, 813–817.
Gerard, J.C., Soret, L., Migliorini, A., Piccioni, G., 2013. Oxygen nightglow emissions of Venus: vertical distribution and collisional quenching. Icarus 223, 602–608.
Hedin, A.E., Niemann, H.B., Kasprzak, W.T., Seiff, A., 1983. Global empirical model of the Venus thermosphere. Journal of Geophysical Research 88, 73–83.
Kaye, J.A., 1988. On the possible role of the reaction $O+HO_2\rightarrow OH+O_2$ in OH airglow. Journal of Geophysical Research 93, 285–288.
Keating, G.M., Bertaux, J.L., Bougher, S.W., Cravens, T.E., Dickinson, R.E, Hedin, A.E., Krasnopolsky, V.A., Nagy, A.F., Nicholson, J.Y., Paxton, L.J., von Zahn, U., 1985. Models of Venus neutral upper atmosphere: structure and composition. Advances in Space Research 5, 117–171.
Krasnopolsky, V.A., 1983a. Venus spectroscopy in the 3000-8000 Å region by Veneras 9 and 10. In Venus. In: Hunten, D.M., Colin, L., Donahue, T.M., Moroz, V.I. (Eds.), Univ. Arizona Press, Tucson, AZ, pp. 459–483.
Krasnopolsky, V.A., 1983b. Lightning and nitric oxide on Venus. Planetary and Space Science 31, 1363–1369.
Krasnopolsky, V.A., 2006. A sensitive search for nitric oxide in the lower atmospheres of Venus and Mars: detection on Venus and upper limit for Mars. Icarus 182, 80–91.
Krasnopolsky, V.A., 2010. Venus night airglow: ground-based detection of OH, observations of O_2 emissions, and photochemical model. Icarus 207, 17–27.
Krasnopolsky, V.A., 2011. Excitation of the oxygen nightglow on the terrestrial planets. Planetary and Space Science 59, 754–766.
Krasnopolsky, V.A., 2012. A photochemical model for the Venus atmosphere at 47-112 km. Icarus 218, 230–246.
Krasnopolsky, V.A., Krysko, A.A., Rogachev, V.N., Parshev, V.A., 1976. Spectroscopy of the Venus night airglow from the Venera 9 and 10 orbiters. Cosmic Research 14, 789–795.
Migliorini, A., Grassi, D., Montabone, L., Lebonnois, S., Drossart, P., Piccioni, G., 2012. Investigation of air temperature on the nightside of Venus derived from VIRTIS-H on board Venus-Express. Icarus 217, 640–647.
Migliorini, A., 8 coauthors, 2013. The characteristics of the O_2 Herzberg II and Chamberlain bands observed with VIRTIS/Venus Express. Icarus 223, 609–614.
Montmessin, F., Bertaux, J.-L., Lefèvre, F., Marcq, E., Belyaev, D., Gérard, J.-C., Korablev, O., Fedorova, A., Sarago, V., Vandaele, A.-C., 2011. A layer of ozone detected in the atmosphere of Venus. Icarus 216, 82–85.
Piccioni, G., 12 coauthors, 2008. First detection of hydroxyl in the atmosphere of Venus. Astronomy and Astrophysics 483, L29–L33.
Piccioni, G., Zasova, L., Migliorini, A., Drossart, P., Shakun, A., Garcia Munoz, A., Mills, F.P., Cardesin-Moinelo, A., 2009. Near-IR oxygen nightglow observed by VIRTIS in the Venus upper atmosphere. Journal of Geophysical Research 114, E00B38.
Romanescu, C., Marakov, A., Timmers, H., Kalogerakis, K.S., Copeland, R.A., 2009. Temperature Dependence of the Vibrational Relaxation of OH($v'=1$ and 2) by CO_2. Abstract #P33A-1270, American Geophysical Union Fall Meeting, San Francisco.
Sander, S.P., 11 coauthors, 2011. Chemical Kinetics and Photochemical Data for Use in Atmospheric Studies. Evaluation no. 17. JPL Publication 10-6.
Seiff, A., 1985. 10 coauthors, 1985. Models of the structure of the atmosphere of Venus from the surface to 100 km altitude. Advances in Space Research 5, 3–58.
Slanger, T.G., Csoby, P.C., Huestis, D.L., Bida, T.A., 2001. Discovery of the atomic oxygen green line in the Venus night airglow. Science 291, 463–465.
Slanger, T.G., Huestis, D.L., Cosby, P.C., Chanover, N.J., Bida, T.A., 2006. The Venus nightglow ground-based observations and chemical mechanisms. Icarus 182, 1–9.
Smith, G.P., Robertson, R., 2008. Temperature dependence of oxygen atom recombination in nitrogen after ozone photolysis. Chemical Physics Letters 458, 6–10.
Soret, L., Gerard, J.C., Piccioni, G., Drossart, P., 2012. The OH Venus nightglow spectrum: intensity and vibrational composition from VIRTIS Venus Express observations. Planetary and Space Science 73, 387–396.
Stewart, A.I.F., Gerard, J.C., Rusch, D.W., Bougher, S.W., 1980. Morphology of the Venus ultraviolet night airglow. Journal of Geophysical Research 85, 7861–7870.
Tellmann, S., 2012. 8 coauthors, 2012. Small-scale temperature fluctuations seen by the VeRa radio science experiment on Venus Express. Icarus 221, 471–480.
Wennberg, P.O., Anderson, J.G., Weisenstein, D.K., 1994. Kinetics of reactions of ground state nitrogen atoms ($^4S_{3/2}$) with NO and NO_2. Journal of Geophysical Research 99, 18839–18846.
Yung, Y.L., DeMore, W.B., 1982. Photochemistry of the stratosphere of Venus: implications for atmospheric evolution. Icarus 51, 199–247.
Zasova, L.V., Moroz, V.I., Linkin, V.M., Khatuntsev, I.V., Maiorov, B.S., 2006. Structure of the Venusian atmosphere from surface up to 100 km. Cosmic Res. 44, 364–383.